X-ray diffraction measurement of layered manganese dioxide that can store/release heat repeatedly by desorbing/absorbing water molecules to/from moist air —Discovery of thermal storage materials that can utilize low-temperature waste heat—

Norihiko L. Okamoto*, Takuya Hatakeyama**, Hongyi Li* and Tetsu Ichitsubo*

Abstract

We have discovered that layered manganese dioxide (birnessite, δ-MnO_2) can store/release heat through an intercalation mechanism in which water molecules in a moist atmosphere are deintercalated/intercalated between the layers. The material has been found to have an excellent balance of various properties required for thermal storage materials, such as low heat-storage temperature, high thermal energy density, good charge/discharge rate, and cyclic properties. In this note, the high-temperature stability of layered manganese dioxide and the crystal structure change accompanying intercalation/deintercalation of water molecules are analyzed by in-situ X-ray diffraction measurements, and its thermal storage properties are evaluated by thermogravimetric differential thermal analysis and differential scanning calorimetry.

1. Introduction

Thermal storage materials, which can store surplus heat energy and release it as needed, have several different types, including sensible heat, phase-change, chemical reaction, and chemisorption[1]–[6]. A familiar example of a chemical-reaction-type heat storage material is a disposable heat pack, which generates heat by oxidizing and hydrating iron. After reducing iron oxide at high temperatures, it is sealed to prevent exposure to the atmosphere (heat-stored state) and can be opened on demand to react with oxygen and moisture in the atmosphere to generate heat (heat-released state). However, although such chemical-reaction and chemisorption types that utilize an oxidation and hydration reaction have a high heat storage energy density, their heat-storing (i.e., charging) temperature is too high and, furthermore, they lack cyclability and reversibility due to deliquescence and large volume distortion by including a large amount of water molecules[2],[7]–[12]. Phase-change materials using sensible heat or latent heat show excellent reversibility of heat absorption/release but have low heat storage energy density and difficulty in maintaining the heat-stored state[3],[5]. Therefore, a new material with a new heat storage mechanism that has all the properties required for heat storage materials (low charging temperature, high heat-storage energy density, good charge/discharge rate property, good cyclability, environmental compatibility, etc.) is desired for reversible use of low-temperature waste heat.

Based on our previous study on the phase stabilities of various polymorphs of manganese dioxide (MnO_2) with different crystal structures[13], we have demonstrated that the layered manganese dioxide (birnessite, δ-MnO_2) shown in Figure 1(a) can be used as a high-performance thermal storage material possessing the above properties[14]. In addition, it has

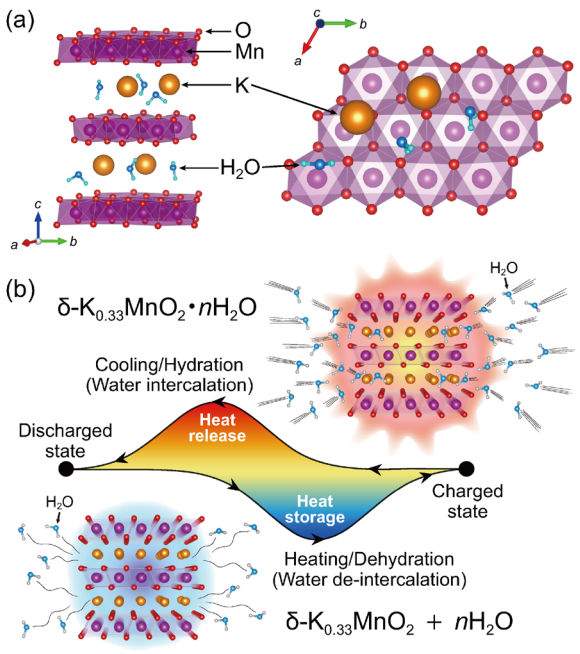

Fig. 1. (a) Crystal structure of layered manganese dioxide δ-$K_{0.33}MnO_2 \cdot nH_2O$. (b) Schematic illustration of the heat storage and release reactions by the water-molecule deintercalation/intercalation mechanism.

* Institute for Materials Research, Tohoku University.
** Graduate School of Engineering, Tohoku University.

also been found that the heat release and absorption reactions of layered manganese dioxide are caused by an intercalation mechanism in which water molecules in the moist atmosphere are inserted into and removed from the interlayer of MnO_6 (Figure 1(b)), which we call "intercalation".

In this technical note, we present our recent study on the high-temperature stability of layered manganese dioxide and the crystal structure change associated with deintercalation and intercalation of water molecules, which were analyzed by X-ray diffraction measurements. Furthermore, we also present excellent thermal storage properties, which were evaluated by thermogravimetric differential thermal analysis (TG-DTA) and differential scanning calorimetry (DSC).

2. Thermal Stability of δ-MnO_2 at High Temperatures

Layered manganese dioxide (δ-MnO_2) was obtained by pyrolysis of potassium permanganate ($KMnO_4$) at 700°C in air[14]–[16]. Inductively coupled plasma (ICP) emission spectroscopy confirmed that the chemical composition was $K_{0.33}MnO_2$ (excluding water molecules), proving that such manganese dioxide obtained by pyrolysis contained potassium[14].

In-situ high-temperature X-ray diffraction measurements of layered manganese dioxide were performed under atmospheric conditions from room temperature to 650°C using SmartLab with a multipurpose high-temperature sample heating stage (Rigaku)[13]. A Mo Kα beam was used as the X-ray source, and a 2θ range from 4 to 34° was measured in continuous mode at a scan rate of 1°/min. Diffraction measurements were performed by increasing the temperature at a rate of 5°C/min and maintaining the temperature isothermally at each measurement temperature. As shown in Figure 2(a), the diffraction peaks (~5.5°, ~11.5°, etc.) coming from the layered manganese dioxide shifted to the higher angle side when the temperature was increased above 150°C. This indicates that the lattice constant decreases with increasing temperature while maintaining the fundamental structure, suggesting that the water of crystallization is desorbed during heating. Furthermore, the diffraction peaks (~8°, ~13°, etc.) attributed to Mn_3O_4 appear when the temperature is raised above 500°C and their diffraction intensities increase with increasing temperature. Namely, at high temperatures, the layered manganese dioxide is subjected to a following reductive decomposition as

$$MnO_2 \rightarrow \frac{1}{3}Mn_3O_4 + \frac{1}{3}O_2\uparrow \quad (1)$$

After cooling to near room temperature (50°C) the structure never reverts to its original state. Diffraction peaks originating from the layered manganese dioxide disappeared while diffraction peaks from Mn_3O_4 became prominent, suggesting that reductive decomposition progressed during cooling.

The stability of the layered manganese dioxide at high temperatures was also investigated by differential

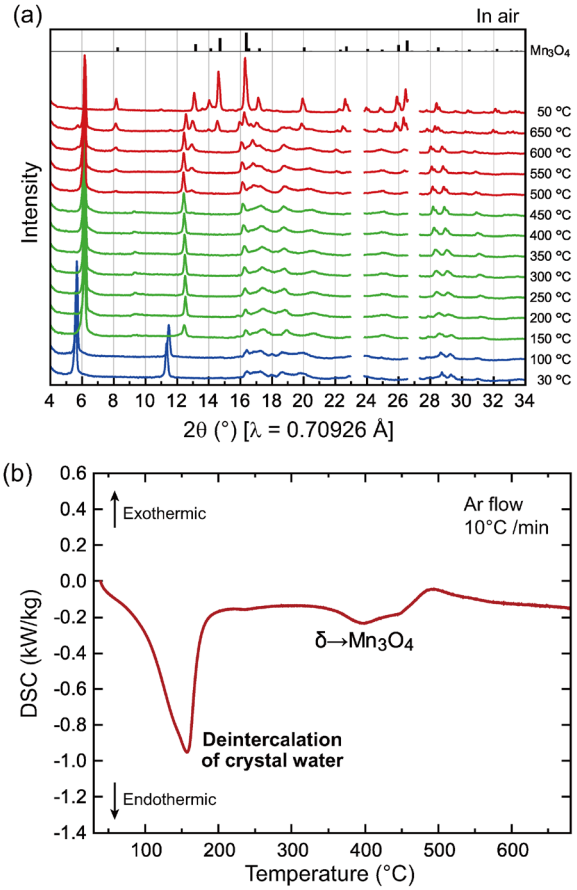

Fig. 2. (a) High-temperature XRD diffraction profiles measured for the layered manganese dioxide under atmospheric conditions and (b) DSC profiles measured in an argon gas flow.

scanning calorimetry (DSC)[13]. Figure 2(b) shows the results of DSC measurements using a heat-flux-type DSC apparatus at a heating rate of 10°C/min in an argon gas flow, and a large endothermic reaction with a peak around 160°C was observed. Such a large endothermic reaction is not observed in other MnO_2 polymorphs (α, β, γ, and λ types), but is specifically observed in δ-(K)MnO_2 containing a large amount of water of crystallization[13]. This suggests that this endothermic reaction is caused by deintercalation of water of crystallization. A relatively indistinct endothermic reaction is observed around 400°C, which corresponds to the reductive decomposition reaction to Mn_3O_4 observed in the high-temperature X-ray diffraction measurement in Figure 2(a). The reason why the onset temperature of reductive decomposition (~400°C) is lower than that of the high-temperature X-ray diffraction measurement (~500°C) is due to the lower oxygen partial pressure in the DSC measurement.

3. High-temperature X-ray Diffraction Measurements of Layered Manganese Dioxide Under Wet and Dry Atmospheres

In order to investigate the structural changes during heating and cooling below the reductive decomposition temperatures, in-situ high-temperature X-ray diffraction

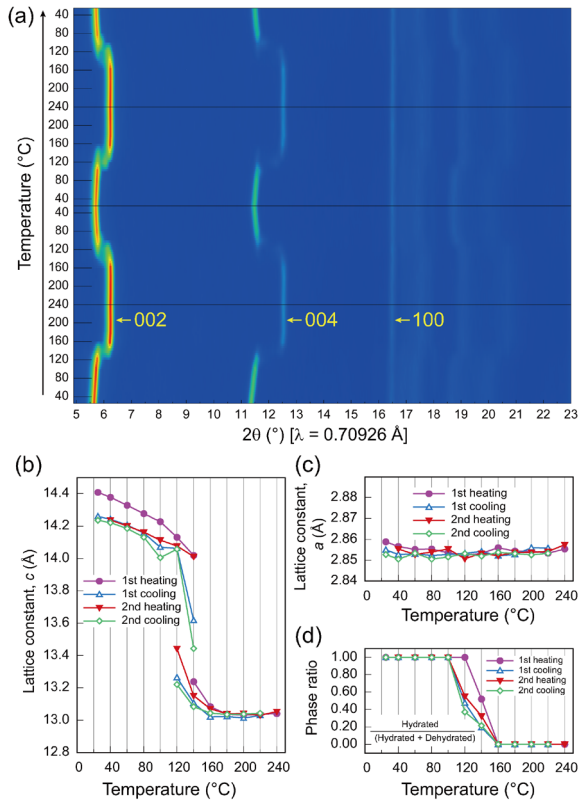

Fig. 3. In-situ high-temperature X-ray diffraction measurements in humid air (60% relative humidity, 25°C). (a) Diffraction intensity color map, (b) *c*-axis lattice parameter, (c) *a*-axis lattice parameter, and (d) temperature dependence of phase ratio of the hydrated phase.

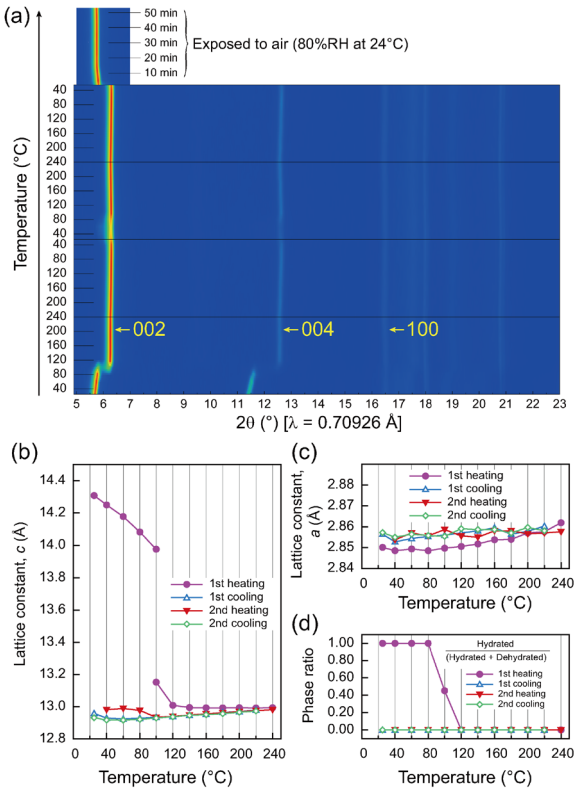

Fig. 4. In-situ high-temperature X-ray diffraction measurements in dry nitrogen. (a) Diffraction intensity color map, (b) *c*-axis lattice parameter, (c) *a*-axis lattice parameter, and (d) temperature dependence of phase ratio of the hydrated phase.

measurements were performed under wet (atmospheric) conditions and dry atmospheres[14].

First, the X-ray diffraction measurements with heating–cooling cycles were performed in air at a relative humidity of 60% (24°C, partial water vapor pressure of 18 hPa). Figure 3(a) shows the color map of the diffraction intensity. The diffraction angles of the 002 and 004 reflections of the layered manganese dioxide gradually increase with increasing temperature, followed by a discontinuous increase at around 140°C. During cooling, the diffraction angles decrease discontinuously around 160°C and further decrease below that temperature. On the other hand, the diffraction angle of the 100 reflection around 16.5° is invariant regardless of temperature. The temperature dependence of the *c*-axis lattice constant (twice the MnO_6 interlayer distance) and the *a*-axis lattice constant calculated from the diffraction angles of the 00*l* and 100 reflections are shown in Figures 3(b) and 3(c), respectively. In the temperature range of 120–140°C, the peaks of the 00*l*-series reflections split, indicating the coexistence of a hydrated phase containing water of crystallization and a dehydrated phase not containing it. Figure 3(d) shows the temperature dependence of the phase ratio of the hydration phase calculated from the intensity of the split 00*l*-series reflection peaks. It is interesting to note that the *c*-axis lattice constant changes with the phase ratio. The *c*-axis lattice constant of the completely dehydrated phase is about 13.0 Å. However, when measured at 120°C during the second heating cycle, where its phase ratio is about 40%, the *c*-axis lattice constant shows a significantly larger value, 13.4 Å. Conversely, the *c*-axis lattice constant of the hydrated phase at 140°C during the second cooling cycle, where its phase ratio is 20%, is 13.4 Å, which is much smaller than that of the fully hydrated phase (14.0–14.4 Å). This indicates that the water molecules in the crystal grains are heterogeneous and that the hydrated and dehydrated phases, which have different interlayer distances, are coherently formed to maintain their overall layered structure. Namely, this large expansion and shrinkage is considered to be a lattice mismatch strain effect.

On the other hand, under a dry nitrogen atmosphere, as shown in Figure 4(a)–(c), after the *c*-axis lattice constant is decreased due to the dehydration reaction during the first-cycle heating, the *a*- and *c*-axis lattice constants remained virtually unchanged even after repeating heating and cooling processes. However, after two cycles, when the sample was exposed to an atmosphere with 80% relative humidity (24°C, water vapor partial pressure 24 hPa), the interlayer distance returned to its original value within a few minutes. This also indicates that the change in interlayer distance during heating and cooling is due to the deintercalation and intercalation of water molecules.

4. Analysis of Deintercalation and Intercalation Behavior of Water Molecules by TG-DTA Measurements in a Humidity-controlled Atmosphere

TG-DTA measurements were performed to investigate the rate and cycling characteristics of the deintercalation and intercalation behavior of water molecules in the layered manganese dioxide[14]. For the measurements, the Thermo plus EVO2 TG-DTA8122/HUM-1 (Rigaku) was used. Six cycle tests were conducted in a humid nitrogen gas atmosphere with a controlled relative humidity of 70% (25°C) at various heating rates of 10, 20, 40, 60, 80, and 100°C/min (Figure 5(a)). Subsequently, the heating rate was set to 20°C/min for 10 cycles (Figure 5(b)). The cooling rate was fixed at 5°C/min for all 16 cycles.

The endothermic reaction during heating was accompanied by a decrease in weight and the exothermic reaction during cooling was accompanied by an increase in weight, which indicates that the endothermic reaction observed in Figure 2(b) at around 160°C was associated with the deintercalation of water molecules. The weight of the sample decreased by about 13% during the first cycle, but the weight did not completely recover even after lowering the temperature. The weight loss during the second and subsequent cycles was about 8%. Assuming that all the water of crystallization is released at 260°C to form $K_{0.33}MnO_2$, the molecular weight of water in the as-synthesized sample is 0.83 mol per $K_{0.33}MnO_2$ composition ($K_{0.33}MnO_2 \cdot 0.83H_2O$). It was estimated to be 0.50 mol ($K_{0.33}MnO_2 \cdot 0.50H_2O$) in the hydrated state after the second cycle. Dehydration was completed at about 190–200°C even when the heating rate was as high as 100°C/min, which was slightly higher than the dehydration completion temperature of 160–170°C at 10°C/min. The fact that the dehydration is completed within 2 minutes at the highest heating rate indicates that the diffusion of water molecules within the material is extremely rapid. As shown in Figure 5(b), the changes in the TG-DTA values followed almost the same trajectory from the 7th to the 16th cycle, indicating that the cycle characteristics were also excellent.

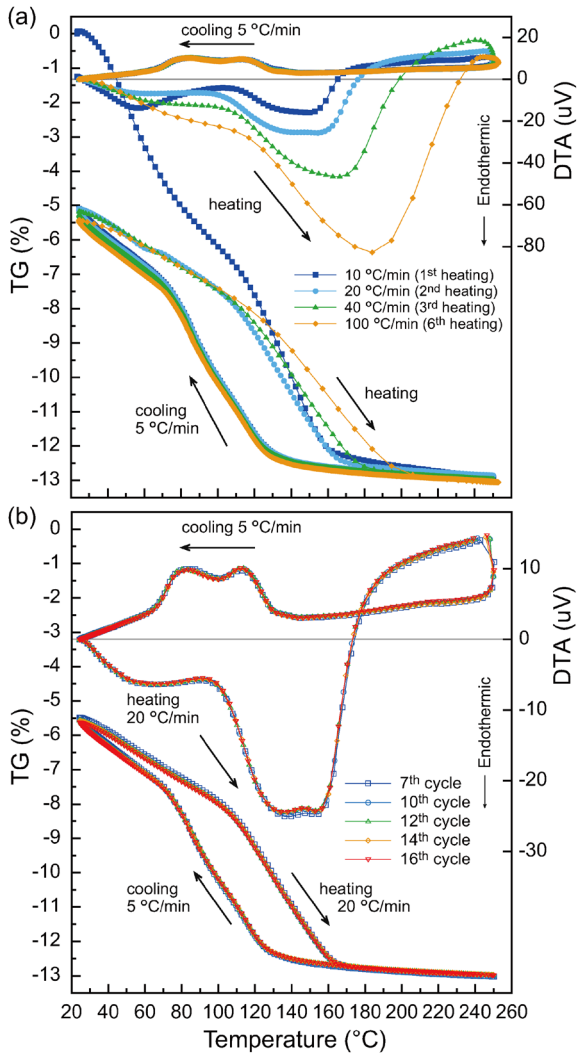

Fig. 5. TG-DTA measurements under a moist nitrogen gas atmosphere controlled at 70% relative humidity (25°C) for (a) rate characteristics (1–6 cycles), (b) cycle characteristics (7–16 cycles).

5. Evaluation of Heat Storage Energy Density by Differential Scanning Calorimetry

To estimate the amount of endothermal energy and thus the heat-storage-energy density associated with the deintercalation of water molecules, DSC measurements were conducted using a heat-flux-type DSC at a heating rate of 5°C/min in an argon gas flow[14]. When the sample was heated up, a large endothermic peak with a shoulder was observed around 40–80°C (open green circles in Figure 6). However, no endothermic peak was observed when the material was heated again in the argon gas flow for a second cycle without exposure to air (open blue squares). After 30 minutes of exposure to air at room temperature, when the temperature was increased in argon gas flow, the endothermic peak

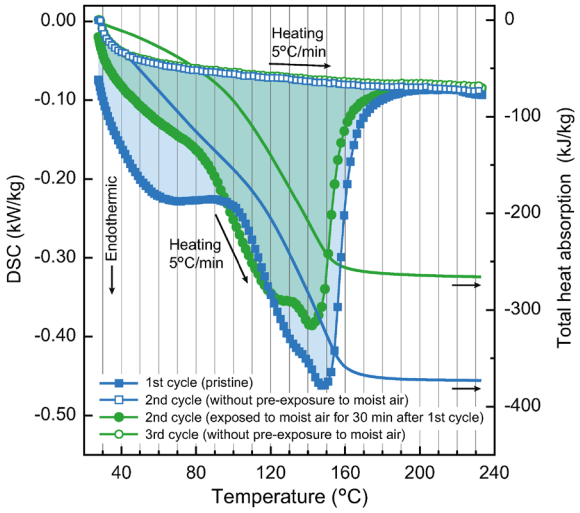

Fig. 6. DSC curves for the layered manganese dioxide and temperature dependence of cumulative endothermic value.

appeared again (filled green circles), but there was no shoulder around 40–80℃ as seen in the first cycle. The initial endothermic capacity (heat absorption amount) of the sample was 373 kJ/kg, calculated from the difference area (blue shaded area) of the DSC curves. On the other hand, the heat absorption after exposure to air was 266 kJ/kg, which was lower than the initial value. This may be due to the irreversible release of excess water of crystallization during the first heating, which appeared as excess heat absorption (a shoulder around 40–80℃). As shown in Figure 3(b), the *c*-axis lattice constant does not return to the initial value (14.4 Å) even after heating and cooling, which is due to this irreversible release of a part of the water of crystallization (0.83 − 0.50 = 0.33 mol).

Using the lattice constants obtained in Section 3, the mass densities of δ-$K_{0.33}MnO_2 \cdot 0.83H_2O$ in the initial state and δ-$K_{0.33}MnO_2 \cdot 0.50H_2O$ containing only reversible water molecules after the second cycle were estimated to be 3740 and 3588 kg/m^3, respectively. Thus, the maximum (initial) and reversible (after the initial cycle) heat storage energy densities were estimated to be 1395 and 1007 MJ/m^3, respectively. This volumetric energy density is comparable to commercially available nickel-metal hydride batteries (500–2000 MJ/m^3)[17].

6. Conclusion

In this note, we have analyzed the crystal structure change of layered manganese dioxide during water deintercalation and intercalation by in-situ X-ray diffraction measurements and thermogravimetric differential thermal analysis. The heat can be stored at temperatures as low as 120–160℃, which is so-called "low-grade waste heat"[18], and the heat-storage state can be preserved for a long period by simply dehydrating, drying, and sealing the material. Furthermore, the heat can be released by naturally absorbing moisture from the air at room temperature, which makes it suitable for various applications such as nighttime heating using solar heat stored during the daytime, heating of automobile engines, thermal gradient for thermoelectric conversion, and heat source for storage batteries operating in a medium temperature range.

Acknowledgments

We thank Mr. Satoshi Otake and Mr. Hiroaki Sato (Rigaku Corporation) for the moisture-controlled TG-DTA analysis. This work is a derivative study from a series of cathode-material studies for rechargeable magnesium batteries, which has been supported by the Advanced Low Carbon Technology Research and Development Program (ALCA-SPRING, grant number: JPMJAL1301) of the Japan Science and Technology Agency (JST). One of the authors, T.H. acknowledges support from Graduate Program in Materials Science at Tohoku University and JST SPRING, Grant Number JPMJSP2114.

References

(1) K. E. N'Tsoukpoe, H. U. Rammelberg, A. F. Lele, K. Korhammer, B. A. Watts, T. Schmidt and W. K. L. Ruck: *Appl. Therm. Eng*., **75** (2015), 513–531.
(2) E. Mastronardo, L. Bonaccorsi, Y. Kato, E. Piperopoulos, M. Lanza and C. Milone: *Appl. Therm. Eng*., **120** (2017), 626–634.
(3) J. Paris, M. Falardeau and C. Villeneuve: *Energy. Sour*., **15** (1993), 85–93.
(4) H. Zondag, B. Kikkert, S. Smeding, R. de Boer and M. Bakker: *Appl. Energ*., **109** (2013), 360–365.
(5) H. Tokoro, M. Yoshikiyo, K. Imoto, A. Namai, T. Nasu, K. Nakagawa, N. Ozaki, F. Hakoe, K. Tanaka, K. Chiba, R. Makiura, K. Prassides and S. Ohkoshi: *Nat. Commun*., **6** (2015), 7037.
(6) P. Pardo, A. Deydier, Z. Anxionnaz-Minvielle, S. Rougé, M. Cabassud and P. Cognet: *Renew. Sustain. Energ. Rev*., **32** (2014), 591–610.
(7) Y. Kato, N. Yamashita, K. Kobayashi and Y. Yoshizawa: *Appl. Therm. Eng*., **16** (1996), 853–862.
(8) Y. Kato, R. Takahashi, T. Sekiguchi and J. Ryu: *International Journal of Refrigeration-Revue Internationale Du Froid*, **32** (2009), 661–666.
(9) V. M. van Essen, H. A. Zondag, J. C. Gores, L. P. J. Bleijendaal, M. Bakker, R. Schuitema, W. G. J. van Helden, Z. He and C. C. M. Rindt: *J. Solar Energ. Eng. Trans. ASME*, **131** (2009), 041014.
(10) M. Steiger, K. Linnow, H. Juling, G. Gülker, A. El Jarad, S. Brüggerhoff and D. Kirchner: *Cryst. Growth Des*., **8** (2008), 336–343.
(11) K. G. Sakellariou, G. Karagiannakis, Y. A. Criado and A. G. Konstandopoulos: *Solar Energ*., **122** (2015), 215–230.
(12) K. Korhammer, M. M. Druske, A. Fopah-Lele, H. U. Rammelberg, N. Wegscheider, O. Opel, T. Osterland and W. Ruck: *Appl. Energ.*, **162** (2016), 1462–1472.
(13) T. Hatakeyama, N. L. Okamoto and T. Ichitsubo: *J. Solid State Chem*., **305** (2022), 122683.
(14) T. Hatakeyama, N. L. Okamoto, S. Otake, H. Sato, H. Y. Li and T. Ichitsubo: *Nat. Commun*., **13** (2022), 1452.
(15) A. C. Gaillot, V. A. Drits, A. Plançon and B. Lanson: *Chem. Mater*., **16** (2004), 1890–1905.
(16) A. C. Gaillot, D. Flot, V. A. Drits, A. Manceau, M. Burghammer and B. Lanson: *Chem. Mater*., **15** (2003), 4666–4678.
(17) W. Chen, Y. Jin, J. Zhao, N. Liu and Y. Cui: *Proc. Natl. Acad. Sci. U.S.A*., **115** (2018), 11694–11699.
(18) H. Jarimi, D. Aydin, Z. Yanan, G. Ozankaya, X. Chen and S. Riffat: *Int. J. Low-Carbon Technol*., **14** (2019), 44–69.